Supplementary Material

Nano-Palladium Dispersed Double-Shelled Carbon Hollow Nanostructures: A Novel Approach to Store Hydrogen

A Flamina[1], R M Raghavendra[2], Anandh Subramaniam[1] and Raghupathy Yuvaraj[1,]*

[1]Materials Science and Engineering, Indian Institute of Technology, Kanpur, India.

[2]Applied Mechanics and Biomedical Engineering, Indian Institute of Technology, Madras, India.

**Author for correspondence: raghu@iitk.ac.in*

The supplementary material provides the following additional information related to the manuscript: (i) Superimposed X-ray diffraction patterns of C-Pd-rGO-aSiO_2 and DSCH sample, (ii) Transmission electron microscopy images of silica spheres and DSCH nanostructures, (iii) Field-emission secondary electron micrograph of DSCH sample, (iv) Fourier transform infrared spectra of silica before and after calcination, (v) Table for comparing Fourier transform infrared peaks, (vi) Zeta potentials of SiO_2, and aSiO_2, (vii) High-resolution Si 2p X-ray photoelectron spectra of GO-aSiO_2 sample, (viii) Textural properties of the prepared samples, (ix) Pseudo-dispersion (μ) and spillover efficiency (η) calculations and (x) Comprehensive literature review of the hydrogen storage performance of various state-of-the-art samples, along with the present work.

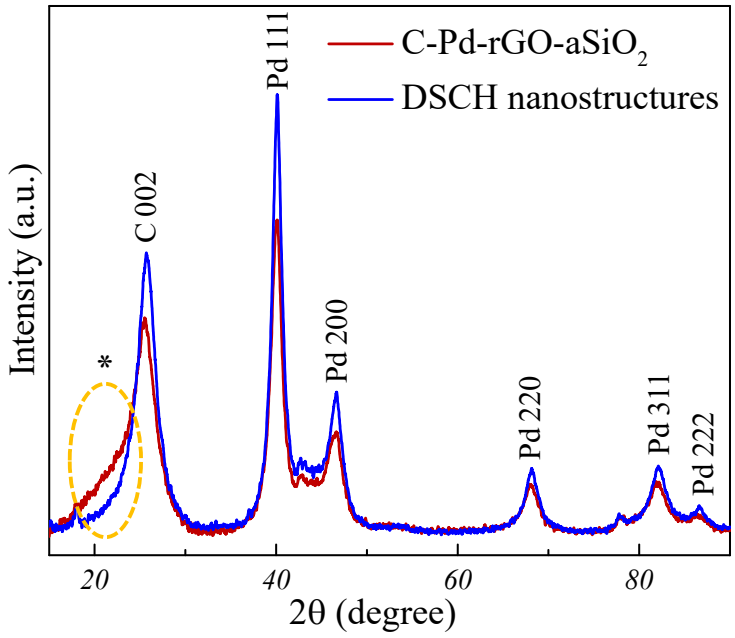

Figure S1. Superimposed X-ray diffractograms of C-Pd-rGO-aSiO_2, and DSCH sample showing the presence of carbon and FCC Pd. However, due to the complete etching of the silica core in the DSCH sample, the broad amorphous hump of silica (*) at $2\theta \approx 22.6°$ disappeared, and only the peak corresponding to the carbon was visible.

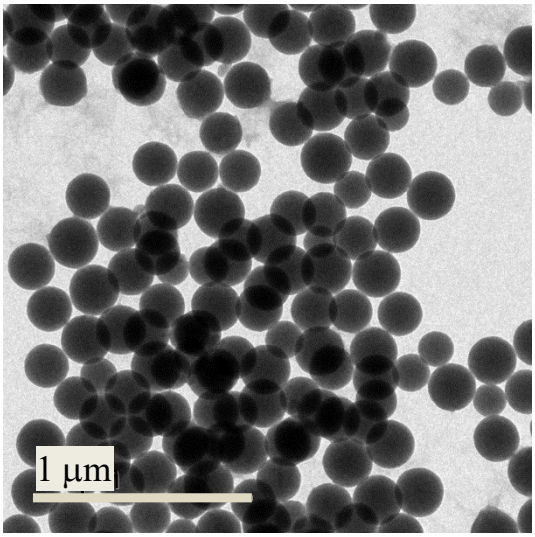

Figure S2. TEM image showing the presence of spherical silica spheres.

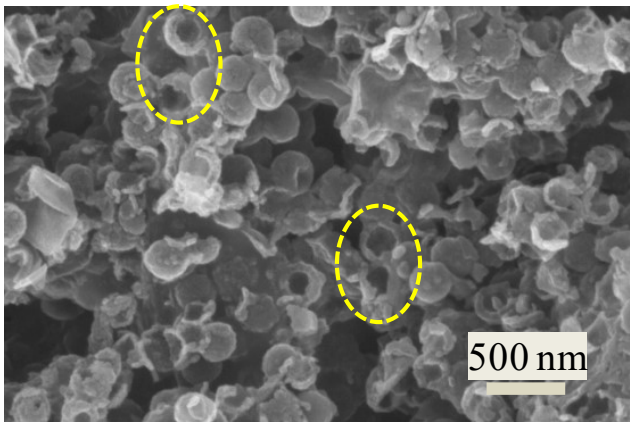

Figure S3. FESEM micrograph of hollow C-Pd-rGO (DSCH) nanostructures revealing the presence of hollow interior from the broken spheres as highlighted in the dashed yellow ellipses.

HRTEM images of DSCH nanostructures confirmed the presence of hollow core after the selective etching of the SiO_2 core and the presence of well-dispersed Pd nanoparticles (average nanoparticle size of ~6.6 nm) within the confined space of the dual shell, i.e. between rGO flakes and porous carbon (Figure S4a-b). The interplanar spacing obtained from the HRLFI is 0.24 nm and corresponds to the (111) planes of Pd (Figure S4c). The hollow core appeared lighter when compared to the shells as seen from the dark field images (DFI) in Figure S4d-e. The EDS elemental mapping of DSCH showed the distribution of C, O and Pd in the sample. The SAED pattern in Figure S3g is indexed to FCC Pd with the rings corresponding to the (111), (200), (220) and (311) planes. An additional observation obtained from the EDS spectra (Figure S4h) is the absence of Si signal, which confirms its complete etching to produce a hollow structure.

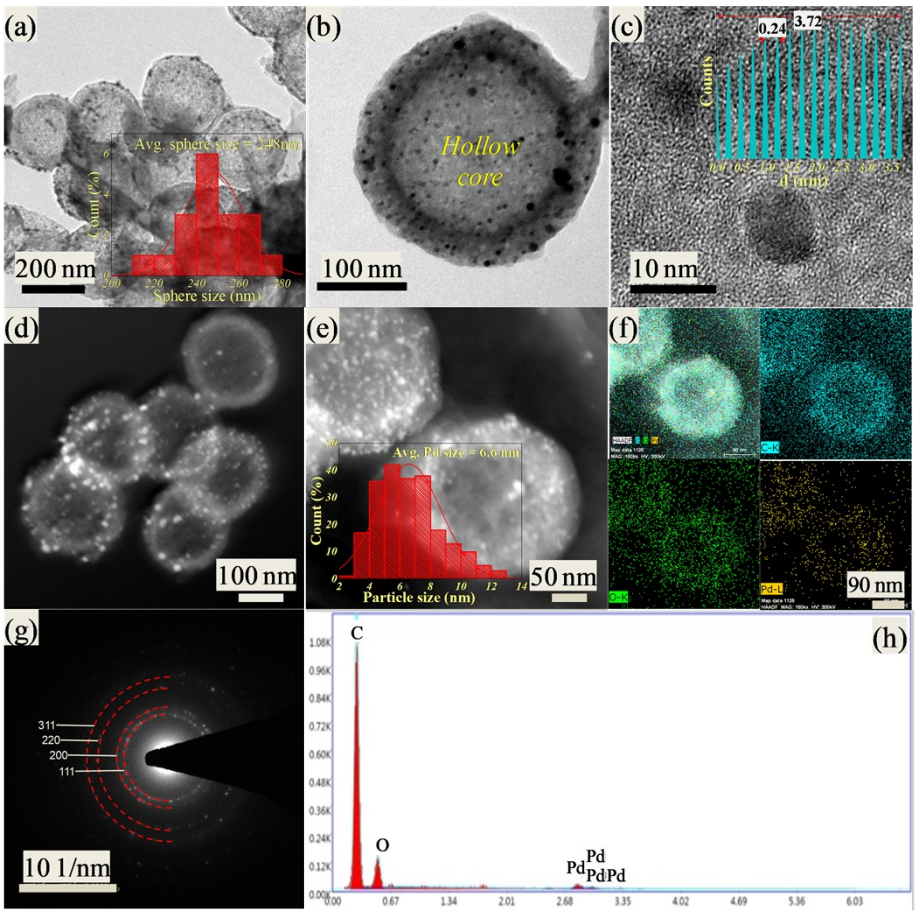

Figure S4. TEM images of DSCH sample showing: (a) Bright field image (BFI) with inset showing the histogram of hollow sphere size distribution, (b) BFI showing the dispersion of Pd nanoparticles in the hollow sphere, (c) HRLFI from a region of the sample showing the (111) crystal planes of Pd (d = 0.24 nm) with inset showing the intensity map, (d) DFI of a group of hollow spheres, (e) High magnification DFI of two hollow spheres with inset showing the histogram of Pd nanoparticles size distribution, (f) EDS map showing layered map and the distribution of O, C and Pd elements, (g) SAED diffraction pattern and (h) EDS spectra showing the presence of only C, O and Pd with the absence of Si element in the sample.

FTIR spectra of silica samples before and after calcination are shown in Figure S5. Both the samples showed the presence of the characteristic Si-O-Si peak at ~1106 cm^{-1}, the major structural backbone of the silica. After calcination, all the peaks were retained with reduced intensity; however, a shoulder peak at ~952 cm^{-1} due to the presence of silanol (Si-OH) group and a weak band at ~1399 cm^{-1} corresponding to the adsorbed ammonia disappeared [1]. The use of mesoporous silica (obtained after calcination) rather than non-porous silica (before calcination) is due to the following reasons. (i) Mesoporous silica has higher surface area (225.2 m^2/g) when compared to non-porous silica (19.8 m^2/g). The higher the surface area, the better the functionalization of the amino group on the silica surface, which is further required for GO

encapsulation. (ii) The presence of porous silica facilitates the complete penetration of the etchant and further aids in its faster etching when compared to the non-porous silica.

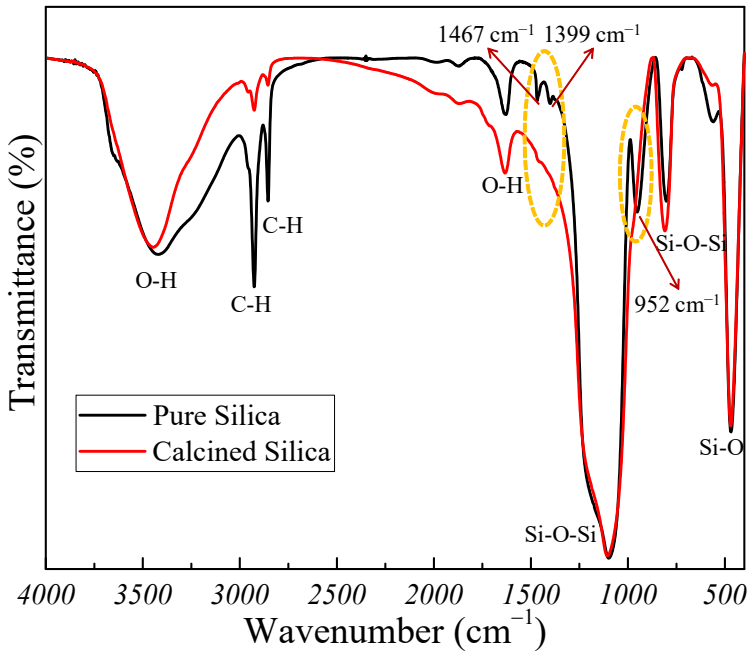

Figure S5. FTIR spectra of silica sample before and after calcination. After calcination, the peaks at ~1399 cm^{-1} and ~952 cm^{-1} corresponding to the presence of adsorbed ammonia and Si-OH bonds disappeared.

The zeta potentials of pristine and functionalized silica spheres were measured to confirm their surface modification by the -NH_2 group. The findings in Table T1 showed that silica has a negative zeta potential of −47.5 mV due to the presence of silanol group. After functionalization with amino-group, the zeta potential was 27.3 mV. This surface modification facilitated the uniform coating of negatively charged GO (−39.6 mV) over the positively charged aSiO_2 surface through electrostatic interaction.

Table T1. Zeta potentials of SiO_2, aSiO_2 and GO measured at pH 6.1.

Sample	Zeta potential (mV)
SiO_2	−47.5
aSiO_2	27.3
GO	−39.6

Table T2. Table listing the FTIR peak positions along with the description of the functional groups and their respective vibration modes.

Wavenumber (cm^{-1})	**Functional group**	**Description**
~3447	O-H	Stretching vibration of adsorbed water molecules
~2926	C-H	Symmetric stretching
~2855	C-H	Asymmetric stretching
~1730	C=O	C=O Stretching vibrations of carbonyl and carboxyl groups
~1632	O-H	Bending vibration of water molecules
~1621	C=C	Skeletal vibration from unoxidized sp^2 CC bonds
~1565	N-H	Bending
~1107	Si-O-Si/SiO-C	Asymmetric Stretching
~1146	C-O	Stretching
~952	Si-OH	Stretching
~809	Si-O-Si	Bending
~468	C-Pd	Stretching

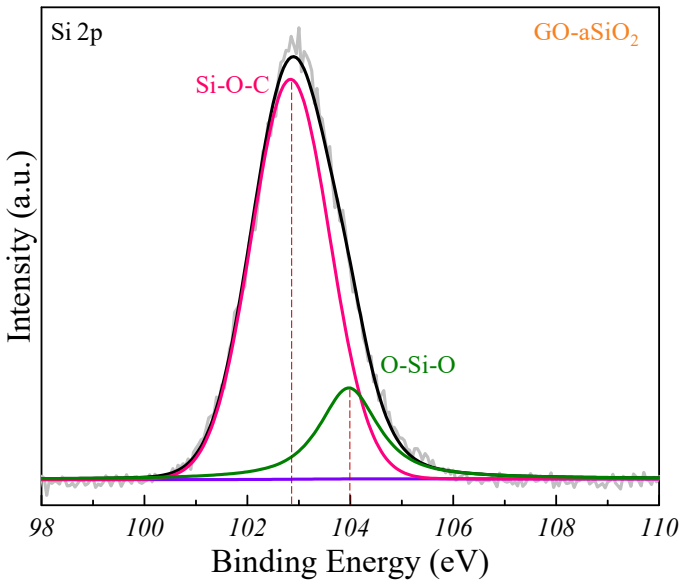

Figure S6. High-resolution Si 2p XPS spectra of GO-$aSiO_2$ sample showing the presence of O-Si-O and Si-O-C.

Table T3. Textural properties of DSCH, C-Pd-rGO-aSiO_2 and hollow Pd-rGO samples.

Sample	No. of Trials	S_{BET} (m^2/g)	V_{total} (cm^3/g)	V_{micro} (cm^3/g)	Pore size (nm)
DSCH nanostructure	1	89.4	0.29	0.10	0.8 - 5.5
	2	87.6	0.27	0.09	0.8 - 5.5
	3	88.2	0.28	0.09	0.9 - 5.4
C-Pd-rGO-aSiO_2	1	84.3	0.25	0.07	0.9 - 5.3
	2	85.7	0.26	0.06	0.9 - 5.3
	3	86.0	0.20	0.08	0.9 - 5.5
Hollow Pd-rGO	1	55.6	0.13	0.05	0.9 - 5.6
	2	53.2	0.11	0.05	1.1 - 5.5
	3	55.9	0.13	0.04	0.9 - 5.6

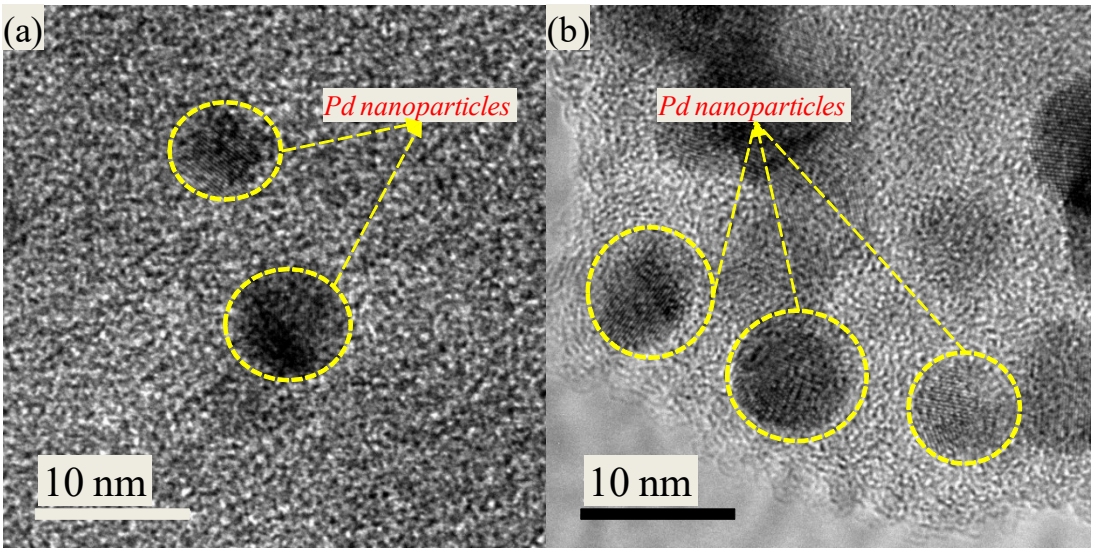

Figure S7. High-resolution TEM images (a) and (b) showing the porosity in DSCH nanostructures obtained at different regions. Pd nanoparticles are shown with dashed yellow circles.

The pseudo-dispersion (μ) and spillover efficiency (η) computed for hollow C-Pd-rGO (DSCH) sample is shown in Table T4. The hydrogen sorption data obtained at a pressure of 0.4 atm and a temperature of 298 K was used in the computation [2,3]. Similar procedure was followed for obtaining the spillover efficiency of hollow Pd-rGO sample.

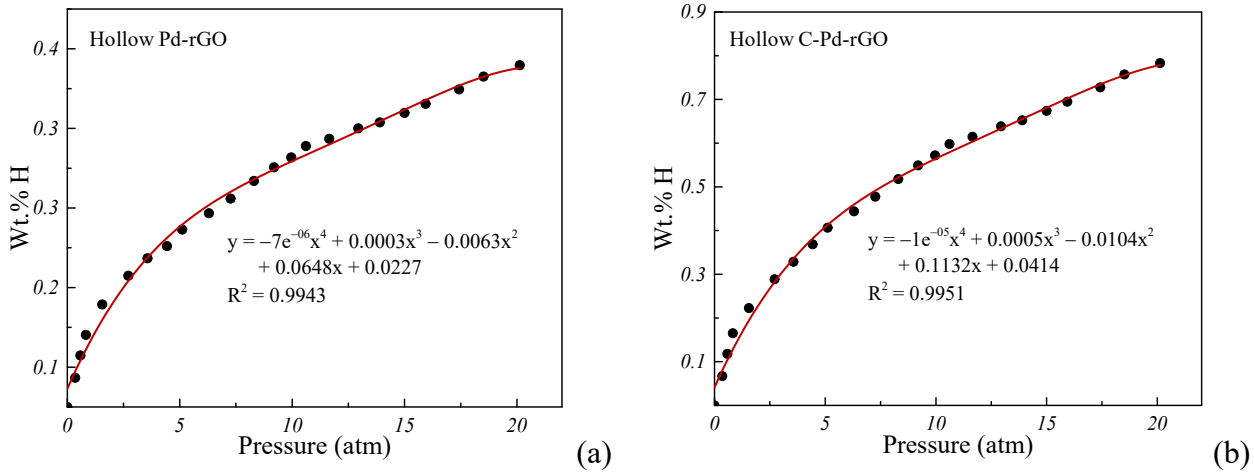

Figure S8. Polynomial curve fitting of the sorption isotherms measured at 298 K and 20 atm for: (a) hollow Pd-rGO, and (b) hollow C-Pd-rGO (DSCH) samples for calculation of pseudo-dispersion (μ) and spillover efficiency (η).

1 Table T4. Pseudo-dispersion (μ) and spillover efficiency (η) calculation for the hollow C-Pd-rGO or
2 the DSCH sample using sorption isotherm obtained at 298 K and 0.4 atm hydrogen pressure.

	Data and computations	Comments
1	DSCH sample: 0.0414 wt.% H_2 = 0.083 mg/g (0.083 mg of hydrogen per gram of sample). Sorption: (0.083 /1.008 g/mol of H) = 0.082 mmol	At 298 K and 20 atm, the sample stores 0.78 wt.%.
2	Amount of Pd in DSCH sample: 5.5 wt.% Pd = 11 mg/g (11 mg of Pd per gram of sample).	Wt.% of Pd determined using EDS technique.
3	Total amount of Pd: 11×10^{-3} g / 106.42 g/mol Pd = 0.103 mmol Pd	-
4	Pseudo-dispersion (μ) = (Sorbed Hydrogen) / (Total Pd) = (0.082 mmol Hydrogen / 0.103 mmol Pd) x 100 = **79.6 %**	The high value of pseudo-dispersion is to be noted.
5	*d* (Particle Size) = 6.6 nm, v_m = 0.0147 nm^3 a_m = 0.0793 nm^2. D = 0.17	Particle size determined from TEM. $D = N_S / N_T$ = No. of surface atoms / Total no. of atoms. v_m = volume occupied by bulk atoms [nm^3], a_m = area occupied by surface atoms [nm^2]. $D = 6\left(\frac{v_m / a_m}{d}\right)$ [4]
6	Spillover efficiency (η) = μ / D = (79.6%) / (17%) = **468%**	η > 100% implies hydrogen storage by spillover effect.

3

Table T5. Hydrogen storage capacity of various pristine and metal-doped carbon materials at an operating temperature and pressure of 298 K and ~20 bar, respectively, as reported in the literature.

Material	T (K)	P (bar)	Wt.% H	Ref.
CNT	298	20	0.8	[5]
Ni supported AC	298	20	0.29	[6]
Ni doped activated carbon nanofibers	298	20	0.55	[7]
C-Ni nanocomposite	298	20	0.73	[8]
Pt decorated nanoporous graphene	298	20	0.131	[3]
Pd decorated nitrogen doped graphene	298	20	1.9	[9]
Nitrogen doped graphene	298	20	1.1	
V doped CNT	298	20	0.69	[10]
Pd doped CNT	298	20	0.66	
Activated MWCNTs	298	21	0.82	[11]
Co loaded activated MWCNTs	298	21	1.06	
Li loaded activated MWCNTs	298	21	1.33	
Ti doped MWCNTs	298	20	1.88	[12]
Ni doped MWCNTs	298	20	0.298	[13]
AC cross-linked polymer composite	298	20	0.17	[14]
Pd_4Hg alloy decorated carbon foam	298	20	5	[15]
Self-aligned GO	298	20	2.5	[16]
Pt doped graphite nanofibers	300	20	<0.1	[17]
Pt loaded MWCNTs	298	20	0.013	[18]
Co doped MWCNTs	298	21	1.06	[19]
Li doped MWCNTs	298	21	1.33	
Pt based HCP	298	19	0.21	[20]
Hollow C-Pd-rGO (DSCH nanostructures)	77	20	3.9	Present work
	273		0.4	
	298		0.78	

Key: CNT - Carbon nanotubes, AC - Activated carbon, MWCNT - Multi-walled carbon nanotube, GO - Graphene oxide, HCP - Hypercrosslinked polymer.

Table T6. Hydrogen storage data of different hollow spheres and core-shell structures along with the current work.

Core-shell nanostructures	T (K)	P (bar)	Wt.% H	Ref.
Cobalt-embedded OMC	298	55	0.45	[21]
Pd hollow spheres	298	1	0.61	[22]
Nickel nano hollow spheres	298	140	0.65	[23]
Pd hollow spheres	298	140	1.22	[24]
(Pt-C_{60})@SiO_2	298	10	0.045	[25]
ZIF-8@ZIF-67	77	1	2.03	[26]
ZIF-67@ZIF-8			1.69	
MIL-101@UiO-66	77	1	2.4	[27]
$LiBH_4$-$Mg(BH_4)_2$ - HCNS	553	100	10.8	[28]
MgH_2-Fe-HCS	573	20	5.6	[29]
Core-shell $NaAlH_4$@Ti	453	130	4.0	[30]
OMHCS@Pd	40	35	0.51	[31]
DMHCS	313	20	0.10	[32]
Pd@DMHCS			0.55	
BN hollow spheres	298	100	4.07	[33]
Hollow nitrogen containing CS	298	80	2.21	[34]
Pd embedded HCS	298	24	0.36	[35]
Zn loaded HGM	473	10	3.26	[36]
Cd/CdO hollow microsphere	473	40	1.30	[37]
Li_2NH hollow nanospheres	473	35	6.0	[38]
Mg-Ni double hollow structures	453	20	5.0	[39]
Hollow Sb-ZnO nanosphere	373	50	1.74	[40]
Hollow carbon spheres	298	90	1.23	[41]
Hollow C-Pd-rGO (DSCH nanostructures)	77	20	3.9	Present work
	273		0.4	
	298		0.78	

Key: OMC - Ordered mesoporous carbon, C_{60} - Fullerenes, ZIF - Zeolitic imidazolate frameworks, OMHCS - Ordered mesoporous hollow carbon spheres, DMHCS - Disordered mesoporous hollow carbon spheres, CS - Carbon spheres, HGM - Hollow glass microspheres.

1 **References**

[1] Kamal M.S. Khalil, Leena A. Elkabee, and Brian Murphy. Formation and characterization of different ceria/silica composite materials via dispersion of ceria gel or soluble ceria precursors in silica sols. *Journal of Colloid and Interface Science* **287**: 534–541 (2005). doi:10.1016/j.jcis.2005.02.041.

[2] A. Flamina, R. M. Raghavendra, Anandh Subramaniam. Agarose derived carbon based nanocomposite for hydrogen storage at near-ambient conditions. *Carbon* **230**: 119657 (2024). https://doi.org/10.1016/j.carbon.2024.119657.

[3] Nikolaos Kostoglou, Chi-Wei Liao, Cheng-Yu Wang, Junko N. Kondo,Christos Tampaxis, Theodore Steriotis, et al. Effect of Pt nanoparticle decoration on the H_2 storage performance of plasma-derived nanoporous graphene. *Carbon* **171**: 294-305 (2021). https://doi.org/10.1016/j.carbon.2020.08.061.

[4] Gérard Bergeret, Pierre Gallezot. Particle Size and Dispersion Measurements. Handbook of Heretogeneous Catalysis, 2, Wiley-VCH, pp.738-765, 2008. 10.1002/9783527610044.hetcat0038

[5] Beatrice Adenirana and Robert Mokaya. Low temperature synthesized carbon nanotube superstructures with superior CO_2 and hydrogen storage capacity. J. Mater. Chem. A, 3: 5148-5161 (2015). https://doi.org/10.1039/C4TA06539E.

[6] M. Zieliński, R. Wojcieszak, S. Monteverdi, M. Mercy, and M.M. Bettahar. Hydrogen storage in nickel catalysts supported on activated carbon. *IJHE* **32**: 1024-1032 (2007). https://doi.org/10.1016/j.ijhydene.2006.07.004.

[7] Natthaporn Thaweelap, Praphatsorn Plerdsranoy, Yingyot Poo-arporn, Patcharaporn Khajondetchairit, Suwit Suthirakun, Ittipon Fongkaew, et al. Ni-doped activated carbon nanofibers for storing hydrogen at ambient temperature: Experiments and computations. *Fuel* **288**: 119608 (2021). https://doi.org/10.1016/j.fuel.2020.119608.

[8] A. Flamina, R. M. Raghavendra, Anandh Subramaniam. Agarose derived carbon based nanocomposite for hydrogen storage at near-ambient conditions. *Carbon* **230**: 119657 (2024). https://doi.org/10.1016/j.carbon.2024.119657.

[9] B.P. Vinayan, K. Sethupathi, S. Ramaprabhu. Facile synthesis of triangular shaped palladium nanoparticles decorated nitrogen doped graphene and their catalytic study for renewable energy applications. *International Journal of Hydrogen Energy* **38**: 2240-2250 (2013). https://doi.org/10.1016/j.ijhydene.2012.11.091.

[10] Renju Zacharia, Keun Young Kim, A.K.M. Fazle Kibria, Kee Suk Nahm. Enhancement of hydrogen storage capacity of carbon nanotubes via spill-over from vanadium and palladium nanoparticles. *Chemical Physics Letters* **412**: 369-375 (2005). https://doi.org/10.1016/j.cplett.2005.07.020.

[11] Maryam Aghababaei, Ali Asghar Ghoreyshi, Kourosh Esfandiari. Optimizing the conditions of multi-walled carbon nanotubes surface activation and loading metal nanoparticles for enhanced hydrogen storage. *International Journal of Hydrogen Energy* **45**: 23112-23121 (2020). https://doi.org/10.1016/j.ijhydene.2020.06.201.

[12] Sami ullah Rather. Hydrogen uptake of Ti-decorated multiwalled carbon nanotube composites. *International Journal of Hydrogen Energy* **46**: 17793-17801 (2021). https://doi.org/10.1016/j.ijhydene.2021.02.185.

[13] Songül Kaskun, Muhammet Kayfeci. The synthesized nickel-doped multi-walled carbon nanotubes for hydrogen storage under moderate pressures. *International Journal of Hydrogen Energy* **43**: 10773-10778 (2018). https://doi.org/10.1016/j.ijhydene.2018.01.084.

[14] Nour F. Attia, Minji Jung, Jaewoo Park, Se-Yeon Cho, Hyunchul Oh. Facile synthesis of hybrid porous composites and its porous carbon for enhanced H_2 and CH_4 storage. *International Journal of Hydrogen Energy* **45**: 32797-32807 (2020). https://doi.org/10.1016/j.ijhydene.2020.03.004.

[15] George M. Psofogiannakis, Theodore A. Steriotis, Athanassios B. Bourlinos, Evangellos P. Kouvelos, Georgia Ch. Charalambopoulou, Athanassios K. Stubos and George E. Froudakis. Enhanced hydrogen storage by spillover on metal-doped carbon foam: an experimental and computational study. *Nanoscale* **3***:* 933-936 (2011). https://doi.org/10.1039/C0NR00767F.

[16] Mahesh Kumar Yadav, Neeraj Panwar, Shiv Singh, Pradip Kumar. Preheated self-aligned graphene oxide for enhanced room temperature hydrogen storage. *International Journal of Hydrogen Energy* **45**: 19561-19566 (2020). https://doi.org/10.1016/j.ijhydene.2020.05.083.

[17] Puja Jain, Dania A. Fonseca, Erik Schaible, Angela D. Lueking. Hydrogen Uptake of Platinum-Doped Graphite Nanofibers and Stochastic Analysis of Hydrogen Spillover. *J. Phys. Chem. C* **111**(4): 1788-1800 (2007). https://doi.org/10.1021/jp0654922.

[18] Anshu Sharma. Investigation on platinum loaded multi-walled carbon nanotubes for hydrogen storage applications. *International Journal of Hydrogen Energy* **45**: 2967-2974 (2020). https://doi.org/10.1016/j.ijhydene.2019.11.093.

[19] Maryam Aghababaei, Ali Asghar Ghoreyshi, Kourosh Esfandiari. Optimizing the conditions of multi-walled carbon nanotubes surface activation and loading metal nanoparticles for enhanced hydrogen storage. *International Journal of Hydrogen Energy* **45**: 23112-23121 (2020). https://doi.org/10.1016/j.ijhydene.2020.06.201.

[20] Buyi Li, Xin Huang, Ruini Gong, Mengrong Ma, Xinjia Yang, Liyun Liang, Bien Tan. Catalyzed hydrogen spillover for hydrogen storage on microporous organic polymers. *IJHE* **37**:12813-12820 (2012). https://doi.org/10.1016/j.ijhydene.2012.05.106.

[21] Chen-Chia Huang, Yi-Hua Li, Yen-Wen Wang, and Chien-Hung Chen. Hydrogen storage in cobalt-embedded ordered mesoporous carbon. *IJHE* **38**: 3994-4002 (2013). http://dx.doi.org/10.1016/j.ijhydene.2013.01.081.

[22] Suboohi Shervani, Puspal Mukherjee, Anshul Gupta, Gargi Mishra, Kavya Illath, T.G. Ajithkumar, Sri Sivakumar, Pratik Sen, Kantesh Balani and Anandh Subramaniam, Multi-mode hydrogen storage in nanocontainers. *IJHE* **42**: 24256-24262 (2017), 10.1016/j.ijhydene.2017.07.233.

[23] Anshul Gupta, Suboohi Shervani, Flamina Amaladasse, Sri Sivakumar, Kantesh Balani and Anandh Subramaniam, Enhanced reversible hydrogen storage in nickel nano hollow spheres. *IJHE* **44**: 22032-22038 (2019). 10.1016/j.ijhydene.2019.06.090.

[24] Flamina Amaladasse, Anshul Gupta, Suboohi Shervani, Sri Sivakumar, Kantesh Balani and Anandh Subramaniam, Enhanced reversible hydrogen storage in palladium hollow spheres, *Part. Sci. Technol.* **39**: 617-623 (2020). https:// doi.org/10.1080/02726351.2020.1776433.

[25] Hui Huang, Hengchao Zhang, Yang Liu, Zheng Ma, Hai Ming, Haitao Lia and Zhenhui Kang. (Pt-C_{60})@SiO_2 nanocomposites for convenient chemical hydrogen storage. *J. Mater. Chem.,* **22**: 20153-20157 (2012). https://doi.org/10.1039/C2JM35406C.

[26] Dharmendra K. Panchariya, Rohit K. Rai, E. Anil Kumar, and Sanjay K. Singh. Core–Shell

Zeolitic Imidazolate Frameworks for Enhanced Hydrogen Storage. *ACS Omega* **3**: 167–175 (2018). https://doi.org/10.1021/acsomega.7b01693.

[27] Jianwei Ren, Nicholas M. Musyoka, Henrietta W. Langmi, Brian C. North, Mkhulu Mathe, and Xiangdong Kang. Fabrication of core–shell MIL-101(Cr)@UiO-66(Zr) nanocrystals for hydrogen storage. *IJHE* **39**: 14912-14917 (2014). https://doi.org/10.1016/j.ijhydene.2014.07.056.

[28] Jiaguang Zheng, Zhendong Yao, Xuezhang Xiao, Xuancheng Wang, Jiahuan He, Man Chen, Hao Cheng, Liuting Zhang, and Lixin Chen. Enhanced hydrogen storage properties of highloading nanoconfined $LiBH_4$-$Mg(BH_4)_2$ composites with porous hollow carbon nanospheres. *IJHE* **46**: 852-864 (2021). http://dx.doi.org/10.1016/j.ijhydene.2020.09.177.

[29] Pawan K. Soni, Ashish Bhatnagar, M.A. Shaz. Enhanced hydrogen properties of MgH2 by Fe nanoparticles loaded hollow carbon spheres. *IJHE* **48**: 17970-17982 (2023). https://doi.org/10.1016/j.ijhydene.2023.01.278.

[30] Chulaluck Pratthana, Kondo-Francois Aguey-Zinsou. Tuning the hydrogen thermodynamics of $NaAlH_4$ by encapsulation within a titanium shell. *IJHE* **48**: 29240-29255 (2023). https://doi.org/10.1016/j.ijhydene.2023.04.028.

[31] Beata Zielinska, Beata Michalkiewicz, Xuecheng Chen, Ewa Mijowska, and Ryszard J. Kalenczuk. Pd supported ordered mesoporous hollow carbon spheres (OMHCS) for hydrogen storage. *Chemical Physics Letters* **647***:* 14–19 (2016). https://doi.org/10.1016/j.cplett.2016.01.036.

[32] Martyna Baca, Krzysztof Cendrowski, Paweł Banach, Beata Michalkiewicz, Ewa Mijowska, Ryszard J. Kalenczuk, and Beata Zielinska. Improving hydrogen storage in modified carbon materials. *IJHE* **42**: 30461-30469 (2017). https://doi.org/10.1016/j.ijhydene.2017.10.146.

[33] Gang Lian, Xiao Zhang, Shunjie Zhang, Duo Liu, Deliang Cui and Qilong Wang. Controlled fabrication of ultrathin-shell BN hollow spheres with excellent performance in hydrogen storage and wastewater treatment. *Energy Environ. Sci.,* **5**: 7072-7080 (2012). https://doi.org/10.1039/C2EE03240F.

[34] Jinhua Jiang, Qiuming Gao, Zhoujun Zheng, Kaisheng Xia, Juan Hu. Enhanced room temperature hydrogen storage capacity of hollow nitrogen-containing carbon spheres. *IJHE* **35**: 210-216 (2010). https://doi.org/10.1016/j.ijhydene.2009.10.042.

[35] Karolina Wenelska, Beata Michalkiewicz, Jiang Gong, Tao Tang, Ryszard Kaleńczuk, Xuecheng Chen, Ewa Mijowska. In situ deposition of Pd nanoparticles with controllable diameters in hollow carbon spheres for hydrogen storage. *IJHE* **38**: 16179-16184 (2013). https://doi.org/10.1016/j.ijhydene.2013.10.008

[36] Sridhar Dalai, Vijayalakshmi Savithri, Pragya Shrivastava, Santosh Param Sivam, Pratibha Sharma. Fabrication of zinc-loaded hollow glass microspheres (HGMs) for hydrogen storage. *International Journal of Energy Research* **39**: 585-726 (2015). https://doi.org/10.1002/er.3292.

[37] Waheed S. Khan, Chuanbao Cao, Faheem K. Butt, Zulfiqar Ali, Zahid Usman, Ghulam Nabi, Ayesha Ihsan, Asma Rehman, Irshad Hussain, M. Tanveer, and Sajad Hussain. Hydrogen storage and PL properties of novel Cd/CdO shelled hollow microspheres prepared under NH_3 gas environment. *IJHE* **38**: 2332-2336 (2013). https://doi.org/10.1016/j.ijhydene.2012.11.121.

[38] Lei Xie, Jie Zheng, Yang Liu, Yan Li, and Xingguo Li. Synthesis of Li_2NH Hollow Nanospheres with Superior Hydrogen Storage Kinetics by Plasma Metal Reaction. *Chem. Mater.* **20**(1): 282-286 (2008). https://doi.org/10.1021/cm071517d.

[39] Anshul Gupta, Suboohi Shervani, Pooja Rani, Sri Sivakumar, Kantesh Balani, Anandh Subramaniam. Hybrid hollow structures for hydrogen storage. *IJHE* **45**: 24076-24082 (2020). https://doi.org/10.1016/j.ijhydene.2019.03.273.

[40] Mashkoor Ahmad, Rafi-ud-Din, Caofeng Pan, and Jing Zhu. Investigation of Hydrogen Storage Capabilities of ZnO-Based Nanostructures. *J. Phys. Chem. C,* 114, 6, 2560–2565 (2010). https://doi.org/10.1021/jp100037u.

[41] Jin-Ho Kim, and Kyu-Sung Han. Ni Nanoparticles-hollow Carbon Spheres Hybrids for Their Enhanced Room Temperature Hydrogen Storage Performance. *Journal of Hydrogen and New Energy* **24**: 550-557 (2013). https://doi.org/10.7316/KHNES.2013.24.6.550.